

pubs.acs.org/NanoLett Letter

Regio- and Steric Effects on Single Molecule Conductance of **Phenanthrenes**

Yan Chen, Mingzhu Huang, Qinghai Zhou, Zhen Li, Jing Meng, Mengyuan Pan, Xiang Ye, Taifeng Liu, Shuai Chang,* and Shengxiong Xiao*



Cite This: Nano Lett. 2021, 21, 10333-10340



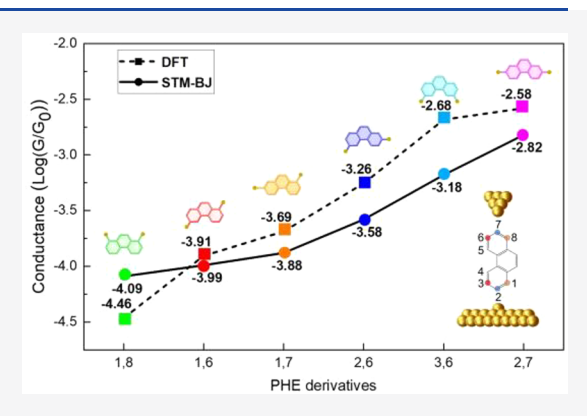
ACCESS I

III Metrics & More

Article Recommendations

Supporting Information

ABSTRACT: Here, six phenanthrene (the smallest arm-chair graphene nanoribbon) derivatives with dithiomethyl substitutions at different positions as the anchoring groups were synthesized. Scanning tunneling microscopy break junction technique was used to measure their single molecule conductances between gold electrodes, which showed a difference as much as 20-fold in the range of $\sim 10^{-2.82}$ G₀ to $\sim 10^{-4.09}$ G₀ following the trend of $G_{2,7} > G_{3,6} > G_{2,6} > G_{1,7} > G_{1,6} > G_{1,8}$. DFT calculations agree well with this measured trend and indicate that the single molecule conductances are a combination of energy alignment, electronic coupling, and quantum effects. This significant regio- and steric effect on the single molecule conductance of phenanthrene model molecules shows the complexity in the practice of graphene nanoribbons as building blocks for future carbon-based electronics in one hand but also provides good conductance tunability on the other hand.



KEYWORDS: phenanthrene, single molecule conductance, regio- and steric effects, STM-BJ, graphene nanoribbons

INTRODUCTION

Carbon-based electronics holds great potential for the next generation electronics beyond Moore's law. 1-5 As the thinnest carbon-based material, graphene has unique electronic structure and electronic properties, 6-10 excellent mechanical strength, good stability, and high carrier mobility. 11 It is considered to be an ideal material for the new generation of micro/nano electronics. 7,12 As a special type of graphene material, graphene nanoribbons (GNRs) are deemed as one of the promising basic building blocks toward the miniaturization of electronic devices and have attracted tremendous research efforts to construct molecular devices. 13-15 With the rapid developments of experimental technology and equipment in molecular electronics, 16-19 molecular or atomic devices based on GNRs have become one of the frontier research focuses. Molecular devices based on GNRs have shown many interesting physical properties, such as molecular rectification, ^{20–22} molecular switching, ^{22–25} negative differential resistance, ^{26,27} spin filtering, ^{21,25} and field effect ^{28–30} characteristics. In the meantime, significant electrical properties ^{31–33} dependence of GNRs on their edge structures presents great opportunities to access materials with suitable characteristics. For example, GNRs with zigzag edges (zGNRs) exhibit metallic characteristics, whereas armchair-shaped GNRs (aGNRs) exhibit semiconductor characteristics.⁶ Polycyclic aromatic hydrocarbons (PAHs), especially polyacenes, represent a special species of short GNRs with atomic precision. Previous studies on the single

molecule conductance of polyacenes can be divided into two categories. When no anchoring groups were applied, electrodemolecule-electrode junctions through van der Waals interactions between the π -orbital of polyacenes and two Ag or Pt electrodes³⁴ or two graphene electrodes³⁵ were constructed. The conductance of Ag/oligoacene junctions first increases with molecule length, followed by the onset of conductance saturation.³⁴ Conversely, the conductance of Pt/oligoacene junctions does not depend on the molecule length.³⁴ In the case of graphene electrodes, the measured exponential dependence of the conductance on the number of benzene rings for linear PAHs with the same number of benzene rings are different.³ Although when anchoring groups are involved, measurements have been limited to how an extension of the acenes along the long axis will affect the conductance perpendicular to the path of tunneling electrons as a function of acene length³⁶ where intermolecular effects and junction geometries play important roles. Another related example by Fujii³⁷ showed that the conductance of heteroatom acenes (pyrazine, quinoxaline, and phenazine) are not only size dependent but also molecular

Received: Revised:

September 14, 2021 November 29, 2021 Published: December 7, 2021





orientation sensitive in the Au-molecule-Au junctions. Still, studies on the regio-effects on the single molecule conductance of PAHs anchored between electrodes are limited to a few examples.^{38–40} Lambert et al.^{38,39} propose a magic ratio rule (MRR) showcasing that the connectivity-driven conductance ratio of graphene-like aromatic molecules is simply the square of the ratio of two "magic integers" whose values depend only on the connectivities to the electrodes. Density functional theory (DFT) calculations results by Palma⁴¹ demonstrate that acene derivatives have near length-independent conductance and the anchoring configuration (steric effect) could dominate the conductance behavior. In general, intrinsic electronic property study of atomically thin GNRs at the single molecule level still presents a great challenge in terms of structure-property interpretations, ^{42–47} and there still lacks a good example to casestudy the regio- and steric effect of anchoring groups on the molecular conductance of GNRs with atomic precision. A systematic case-study of the regio- and steric effect of six phenanthrene derivatives with dithiomethyl substitutions at different positions as the anchoring groups with the same aromatic core is highly desirable.

In this work, we mainly focus on the design, synthesis, and single molecule conductance measurements of the smallest aGNRs unit, phenanthrenes (PHE) (Figure 1). By using a

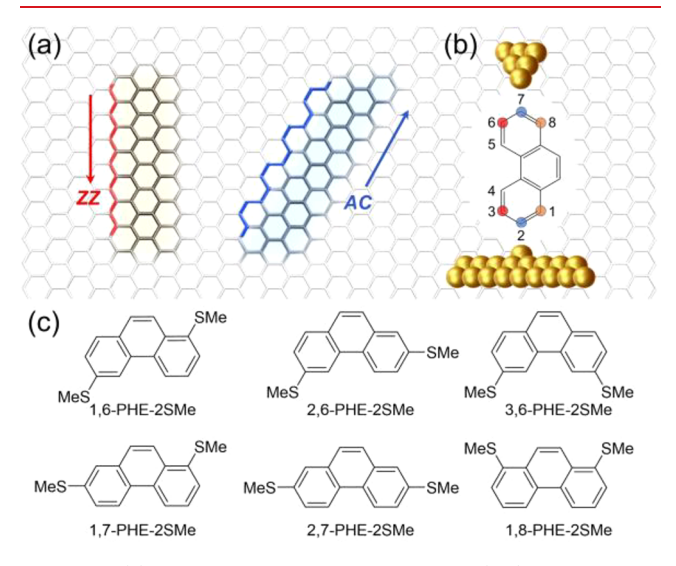


Figure 1. (a) Schematic presentation of zigzag (*ZZ*) and armchair (AC) graphene nanoribbons. Adapted from ref 48. Copyright 2021 Springer Nature Limited. (b) Schematic presentation of STM-BJ single molecule conductance measurement of the smallest aGNR: phenanthrene. (c) Molecular structures of six phenanthrene (PHE) derivatives with two thiomethyl (–SMe) anchoring groups substituted at different positions (PHE-2SMe).

home-built scanning tunneling microscopy break junction (STM-BJ) setup^{49–52} (Figure 1b), a single-molecule charge transport through a series of six phenanthrene molecules by varying the positions of dithiomethyl (SMe) anchor groups (Figure 1c) were investigated. Experimental data and density functional theory (DFT) calculations were examined to explore the influence of both the regio- and steric effects of anchor groups on their electronic properties. Previous theoretical predictions by DFT methods on the transport properties of naphthalene, anthracene, and PHE indicate highly site-dependent characteristic.^{53,54} We found that even with the same molecule core, the different locations of the anchoring groups

would result in significant conductance differences by as much as 20-fold. The important finding is that the anchoring configuration has a predominate effect on the conductance behavior of PHE, which are optimal building blocks to fabricate single-molecule devices with tunable charge transport properties

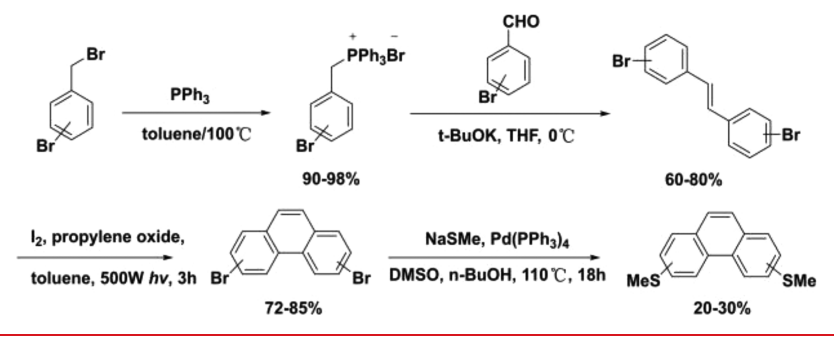
■ RESULTS AND DISCUSSION

All molecules were synthesized following three key reactions (Scheme 1), namely, Wittig olefination to furnish dibromostilbene, oxidative photocyclization of the latter to afford dibromophenanthrene, and Pd-catalyzed Suzuki coupling with NaSMe $^{\rm 55-57}$ to yield final target molecules of dithiomethylphenanthrene (PHE-2SMe) (Section 1 in Supporting Information). The double thiomethylation could be achieved from a Pd-catalyzed reaction of Aryl-Br with CH $_{\rm 3}$ SNa in DMSO/n-BuOH at 100 $^{\circ}$ C. The yields are moderate to high because the Pd insertion into the C–Br bond will facilitate the subsequent substitution of –SMe groups. All of the compounds were characterized by comprehensive spectroscopic data (Figure S1 and NMR Spectra in Supporting Information).

Conductance measurements of these compounds were carried out using STM-BJ technique (see Section 2 in Supporting Information for details). Pure solvent 1,2,4trichlorobenzene (TCB) was used for the measurements, which show a noise level of 10⁻⁵ G₀ (Figure S2). Thousands of current decay traces were recorded for each molecular species with typical raw traces showing conductance steps (or plateaus) presented in Figure S3. Two-dimensional (2D) conductance displacement histograms are constructed by aligning all of the recorded data set (~5000 traces) for each molecule without data selection, and distinctive conductance features can be visually seen in these 2D histograms as shown in Figure 2a-f. The possibility of forming molecular dimer junctions was ruled out by conductance measurement of monosubstituted 2-PHE-SMe molecule, which showed no obvious conductance peak in the range of $10^{-4.7}$ G₀ to 10^{0} G₀ (Figure S4). In Figure 2a, the overlaid conductance plateau for molecule 2,7-PHE-2SMe (2,7) is relatively flat with well-defined electronic conductance and step length, while for molecule 1,7, 1,6, 2,6 (Figure 2b,d,e), the conductance plateaus are very tilted with their conductance ranges extending from 10^{-2} to 10^{-4} G₀. For 1,8 and 3,6, the overlaid plateau is even more tilted. But after data selection, 2D conductance-displacement histograms and conductance histograms for 1,8 (Figure S5a,c) and 3,6 (Figure S5b,d) show a clear conductance peak. All of these electrical behaviors of single molecules with the elongation of the electrode gap distance reflect the unique electrical and mechanical properties of each molecular type.

To gain insight into the structure—property relationship of the six synthesized molecules with subtle structural difference, we systematically compare their single molecule electronic conductance, conductance plateau slope, the percentage of molecular junction formation, and the junction stretching length which are obtained by statistically analyzing each current decay trace (see Figures S7 and S8 for data analysis methods). The results are summarized in Figure 2g—j. Figure 2g shows the combined 1D conductance histograms for six molecules constructed by compiling all of the current decay traces for each molecule without data selection. One-dimensional conductance histograms with data selection for only 1,8 and 3,6 but not the other four derivatives (Figure S9, Table S1) showed much clearer conductance differences. It is essentially

Scheme 1. Synthetic Routes of Dithiomethyl Phenanthrene (PHE-2SMe) Derivatives



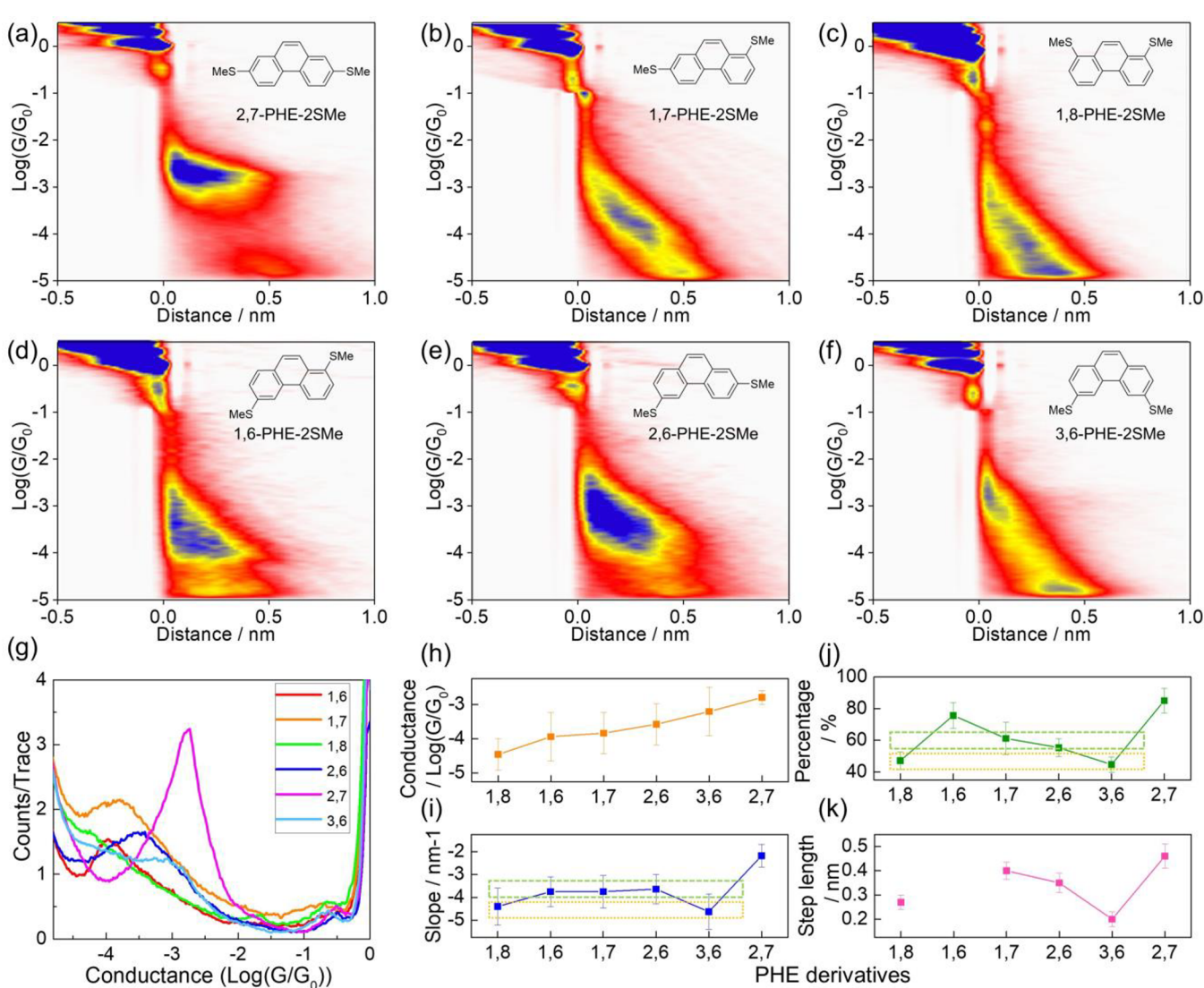


Figure 2. (a–f) Two-dimensional conductance—distance histogram for PHE derivatives showing a clear conductance peak that extends over a distance of 0.5 nm relative to the break of the G_0 contact. A 0.005 nm bin size was used for the distance axes, while the conductance axes feature 50 bins per decade. All traces aligned in a common distance scale by setting the first point with the conductance $G < 0.1 G_0$ to 0 nm. (g) One-dimensional conductance histograms constructed using logarithmic bins for junctions of PHE derivatives. Histograms were generated from over 5000 traces without data selection. (h) Logarithmic plot of single-molecule conductance versus different PHE derivatives from (g). Plot of the (i) conductance plateau slope, (j) the percentage of molecular junction formation, and (k) the junction stretching length of PHE derivatives. The full width at half-maximum of the Lorentz fitting curve (Figure S6) is used for "peak width" for the error bars. Unselected data for 1,8 and 3,6 are used.

the same as Figure 2h where the statistical conductance peaks and peak widths are represented as a scatter point with error bar on top. From both plots, we see a conductance trend of $G_{2,7} > G_{3,6} > G_{2,6} > G_{1,7} > G_{1,6} > G_{1,8}$.

The conductance peak for 2,7 stands out much sharper (and higher) than the other molecules, consistent with the flat conductance plateau seen in Figure 2a. It indicates that the single molecule conductance of 2,7 is not sensitive to the electrode gap

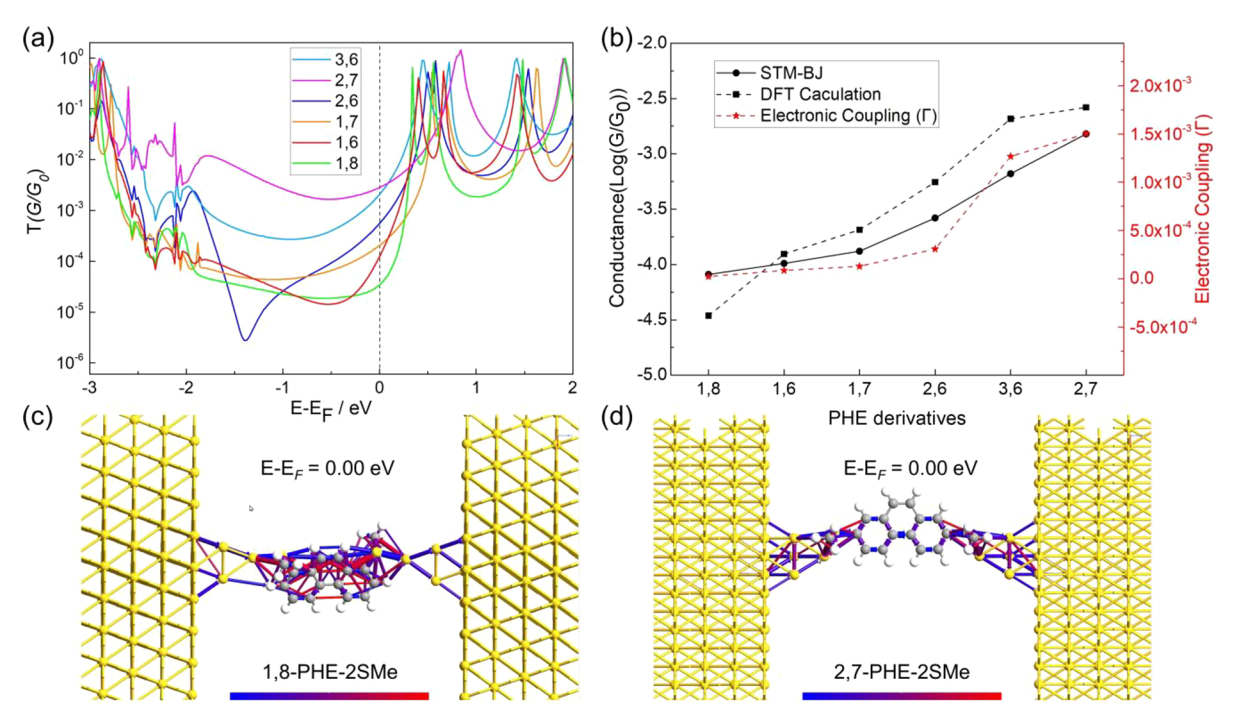


Figure 3. (a) Transmission spectra of dithiomethyl PHE derivatives. (b) Experimental conductance data for dithiomethyl phenanthrene derivatives (black solid line, black axis on the left), compared with DFT calculations (black dashed line, black axis on the left) and electronic coupling (Γ) (red dashed line, red axis on the right). (c) Transmission pathways of 1,8. (d) Transmission pathways of 2,7.

Table 1. Single Molecule Conductance from STM-BJ Experiment and DFT Calculations, Calculated Plateau Length, Orbital Energy Levels, and Electronic Coupling (Γ) of Six PHE Derivatives

molecule	exp. $\log(G/G_0)$	calc. $\log(G/G_0)$	calc. S–S distance (Å) ^a	HOMO eV	LUMO eV	Gap eV	Γ^b eV
1.6-PHE-2SMe	-3.99	-3.91	9.28	-4.76	-2.05	2.72	8.65×10^{-5}
1.7-PHE-2SMe	-3.88	-3.69	9.47	-4.73	-2.00	2.73	1.29×10^{-4}
1.8-PHE-2SMe	-4.09	-4.46	7.50	-4.82	-2.04	2.78	2.35×10^{-5}
2.6-PHE-2SMe	-3.58	-3.26	9.49	-4.72	-1.96	2.76	3.09×10^{-4}
2.7-PHE-2SMe	-2.82	-2.58	10.65	-4.74	-1.97	2.77	1.50×10^{-3}
3.6-PHE-2SMe	-3.18	-2.68	7.51	-4.70	-2.00	2.71	1.27×10^{-3}
^a Measured S-S distance after DFT geometry optimization. ^b Calculated through eq 1 shown below. ³⁷							

distance (Figure S23), which implies that the electronic coupling between the -SMe group and the gold electrode is most stable for 2,7 where the symmetric -SMe groups at two ends of the phenanthrene backbone could stably bridge the undercoordinated gold atoms from two electrodes and form a much durable junction against the molecular stretching. Even though anchoring groups at 1,3,6,8- positions can provide molecular junctions that are mechanically stable, meta linkers do not provide strong electronic coupling into the π -system. Such electronical coupling (Γ) with the electrodes are relatively weaker than para-positioned linker groups such as 2,7. The trend is in fairly good agreement with the conductance values as shown in Figure 3b.

In contrast, the conductance plateau slopes for the other five molecules are much smaller, which however can be separated into two groups, as shown in the orange and green circled regions in Figure 2i. The slopes 1,8 and 3,6 present the largest conductance plateau slopes (most tilted in the 2D histograms shown in Figure 2c,f), indicating that the molecular conductance drops rapidly with the molecular stretching length (Figure S24). This could be explained by their intrinsic chemical feature where the —SMe functional groups are positioned on the side chains of the phenanthrene, in which case their binding configurations

with the gold adatoms can be easily deformed at retraction and the molecule-gold electronic coupling is instantly weakened. Slopes 1,7, 2,6, and 1,6 show an intermediate conductance plateau slope (green circled points in Figure 2i), suggesting a more durable junction than 1,8 and 3,6, but less stable than 2,7. A similar trend is seen in the junction formation percentage for six molecules, as shown in Figure 2j. 1,8 and 3,6 show the smallest occurrence rate for the molecular junction formation, which is unquestionably related to the two closely neighboring -SMe groups positioned on the same side of the phenanthrene. Such a configuration is expected (intuitively) to form a stable monolayer on one electrode surface and pose difficulty to form molecular junctions with undercoordinated gold atoms. 1,7 and 2,6 have a higher binding frequency, showing that a minor shift of the anchor group from meta- to para- position could significantly improve the junction formation rate. 2,7 has the highest junction formation rate over the other molecules with a frequency of up to \sim 85% of all retractions. The rigid chemical structure of phenanthrene and the para-symmetric -SMe groups could both contribute to the high junction formation probability, showing the superiority of using GNRs-based materials as single molecule electronic components. Figure 2k summarizes the stretching length of the conductance plateaus of

each molecule, reflecting the bridging length of six molecules spanning the junction gap. The obtained junction lengths show consistency with the molecular dimensions of different compounds calculated using DFT, as shown in Table 1.

We also performed DFT calculations of all six molecules via nonequilibrium Green's functions (NEGF) (see Section 4 in Supporting Information for calculations details) to better understand which factor contributes more to the single molecule conductance. Calculated conductance, S—S distances, HOMO, LUMO energy levels, and electronic couplings were summarized in Table 1. It is obvious that the conductance is not determined by the S—S distance. The UV—vis absorption spectra of all six PHE derivatives were compared to that of the parent PHE (Figure S10), but no clear trend can be concluded.

$$T(E) = \frac{\Gamma^2}{(E - \varepsilon)^2 + \Gamma^2} \tag{1}$$

Charge transport through a single-molecule junction $^{60-62}$ can be explained using the resonant-level model. In this model, the charge transmission probability is approximately represented as a Lorentzian function 63,64 (eq 1) with the energy difference (ε) between the Fermi level ($E_{\rm F}$) and the energetically closest molecular orbital level (e.g., the lowest unoccupied molecular orbital (LUMO) or the highest occupied molecular orbital (HOMO)), and the electronic coupling between the metal electrodes and a single molecule (Γ).

Figure 3a shows the transmission spectra calculated by DFT. The LUMOs of PHE derivatives are energetically closer to the $E_{\rm F}$ of the metal electrodes. When LUMOs energy levels were applied to eq 1, electronic coupling (Γ) of PHE derivatives is derived and summarized in Table 1. We plotted the measured conductance, calculated conductance, and electronic coupling (Γ) in Figure 3b. The calculated conductance (black dashed line) showed good agreement with the trend of our measured conductance (black solid line). From the transmission pathway of 3,6 shown in Figure S25, the electron transport follows the molecular skeleton, and no obvious reverse electron transport is found. The changes in LUMO energy levels are related to the different substitution sites (regio-effect). The electronic coupling (Γ) is predominantly determined by the molecular conformations in the gold-molecule-gold junctions (steric effect). As shown in Figure 3b, the electronic coupling (Γ) showed a close resemblance of the DFT calculated conductance.

To decipher the transmission mechanism of these conjugated molecule, the optimized junction structures for all derivatives and their transmissions were plotted in Figure S25 and the HOMO and LUMO orbitals are shown in Table S3. The fact that electron-density distributions of the LUMO are mainly located on the backbone of PHE reveals that there are strong electronic coupling interactions among the backbones (Table S3). The colored arrows denote the direction of electron transport, blue arrows represent electron transport from the left electrode to the right one, and red arrows represent electron transport in the opposite direction. In Figure 3a, we found the transmission for 2,6 has an antiresonance in the transmission at \sim -1 to \sim -1.5 eV of the Fermi energy. But this feature is 1.0-1.5 eV below the Fermi energy and does not seem to notably affect the transmission at the Fermi energy. While 1,8 has an antiresonance close to the Fermi energy, indicating a slight suppression of the transmission by destructive quantum interference. The transmission pathways of 1,8 with the lowest measured conductance and 2,7 with the highest measured

conductance are shown in Figure 3c,d, respectively. In 2,7, the electrons are transported along all pathways across the molecular skeleton, while in 1,8, the electrons are mainly transported along the shortest pathway across the skeleton between the two anchor groups. In the meantime, significant electron transport in opposite directions occurs in 1,8, indicating obvious signatures of destructive quantum interference. 13 This also explains the regio-effect of the anchor groups as discussed above. The relatively lower conductance of 1,6, 1,7, and 1,8 with one of the anchoring -SMe groups at the 1position (meta-position to the central benzene ring) are due to the destructive quantum effects (DQI), which are well reported in the literature. $^{58,59,65-68}$ Especially for 1,8, obvious reverse of the ring current can be seen in Figure 3c. On the other hand, the para-positioned linker groups, such as 2,7 can effectively couple across the π -system and provide a conducting single-molecule junction.

CONCLUSION

In summary, we have investigated the regio- and steric effect on the single molecule conductance of phenanthrene model molecules by placing anchors (—SMe) at different positions on the PHE core. STM-BJ measurements and DFT calculation were compared and analyzed. The results demonstrate that substitution at different positions on the phenanthrene core could lead to changes in molecular energy levels and the electronic coupling between gold electrodes. These two factors have a significant impact on transmission function, and single molecule conductance tuning of 20-fold could be obtained by adjusting the contact positions. This work proposes a desirable and convenient method for structural adjustment of conductance at the single-molecule level, which brings new strategies for future application of graphene nanoribbons in the field of carbon-based electronics.

ASSOCIATED CONTENT

Supporting Information

The Supporting Information is available free of charge at https://pubs.acs.org/doi/10.1021/acs.nanolett.1c03565.

Details of materials synthesis, chemicals and electrodes, the STM-BJ setup, and single-molecule conductance measurement, theoretical calculations, NMR spectra, and Mass spec data (PDF)

AUTHOR INFORMATION

Corresponding Authors

Qinghai Zhou — The Education Ministry Key Lab of Resource Chemistry, Joint International Research Laboratory of Resource Chemistry, Ministry of Education, Shanghai Key Laboratory of Rare Earth Functional Materials, College of Chemistry and Materials Science, Shanghai Normal University, Shanghai 200234, China; orcid.org/0000-0002-3593-1521; Email: zhouqh@shnu.edu.cn

Shuai Chang — The State Key Laboratory of Refractories and Metallurgy, the Institute of Advanced Materials and Nanotechnology, Wuhan University of Science and Technology, Wuhan, Hubei 430081, China; orcid.org/0000-0001-7405-5555; Email: schang23@wust.edu.cn

Shengxiong Xiao — The Education Ministry Key Lab of Resource Chemistry, Joint International Research Laboratory of Resource Chemistry, Ministry of Education, Shanghai Key Laboratory of Rare Earth Functional Materials, College of

Chemistry and Materials Science, Shanghai Normal University, Shanghai 200234, China; orcid.org/0000-0002-9151-9558; Email: xiaosx@shnu.edu.cn

Authors

- Yan Chen The Education Ministry Key Lab of Resource Chemistry, Joint International Research Laboratory of Resource Chemistry, Ministry of Education, Shanghai Key Laboratory of Rare Earth Functional Materials, College of Chemistry and Materials Science, Shanghai Normal University, Shanghai 200234, China
- Mingzhu Huang The State Key Laboratory of Refractories and Metallurgy, the Institute of Advanced Materials and Nanotechnology, Wuhan University of Science and Technology, Wuhan, Hubei 430081, China
- Zhen Li The Education Ministry Key Lab of Resource Chemistry, Joint International Research Laboratory of Resource Chemistry, Ministry of Education, Shanghai Key Laboratory of Rare Earth Functional Materials, College of Chemistry and Materials Science, Shanghai Normal University, Shanghai 200234, China
- Jing Meng The Education Ministry Key Lab of Resource Chemistry, Joint International Research Laboratory of Resource Chemistry, Ministry of Education, Shanghai Key Laboratory of Rare Earth Functional Materials, College of Chemistry and Materials Science, Shanghai Normal University, Shanghai 200234, China
- Mengyuan Pan The Education Ministry Key Lab of Resource Chemistry, Joint International Research Laboratory of Resource Chemistry, Ministry of Education, Shanghai Key Laboratory of Rare Earth Functional Materials, College of Chemistry and Materials Science, Shanghai Normal University, Shanghai 200234, China
- Xiang Ye Key Laboratory of Opto-electrical Material and Device, Department of Physics, Shanghai Normal University, Shanghai 200234, China; orcid.org/0000-0002-9034-0046
- Taifeng Liu The Education Ministry Key Lab of Resource Chemistry, Joint International Research Laboratory of Resource Chemistry, Ministry of Education, Shanghai Key Laboratory of Rare Earth Functional Materials, College of Chemistry and Materials Science, Shanghai Normal University, Shanghai 200234, China; occid.org/0000-0003-1943-6229

Complete contact information is available at: https://pubs.acs.org/10.1021/acs.nanolett.1c03565

Author Contributions

Y.C. and M.H. contributed equally.

Notes

The authors declare no competing financial interest.

ACKNOWLEDGMENTS

We acknowledge financial support from the National Natural Science Foundation of China (NSFC) (21772123, 21761142011, 51502173, 21702095), Shanghai Pujiang Program (20PJ1412100), Shanghai Engineering Research Center of Green Energy Chemical Engineering (18DZ2254200), "111" Innovation and Talent Recruitment Base on Photochemical and Energy Materials (D18020), Shanghai Government (21010503400, 18JC1412900) and International Joint Laboratory of Resource Chemistry (IJLRC).

REFERENCES

- (1) Saito, S. Carbon Nanotubes for Next-Generation Electronics Devices. *Science* **1997**, 278 (5335), 77–78.
- (2) Shulaker, M. M.; Hills, G.; Patil, N.; Wei, H.; Chen, H.-Y.; Wong, H. S. P.; Mitra, S. Carbon nanotube computer. *Nature* **2013**, *501* (7468), 526–530.
- (3) Qiu, C.; Zhang, Z.; Xiao, M.; Yang, Y.; Zhong, D.; Peng, L.-M. Scaling carbon nanotube complementary transistors to 5-nm gate lengths. *Science* **2017**, *355* (6322), *271*–*276*.
- (4) Hills, G.; Lau, C.; Wright, A.; Fuller, S.; Bishop, M. D.; Srimani, T.; Kanhaiya, P.; Ho, R.; Amer, A.; Stein, Y.; Murphy, D.; Arvind; Chandrakasan, A.; Shulaker, M. M. Modern microprocessor built from complementary carbon nanotube transistors. *Nature* **2019**, *572* (7771), 595–602.
- (5) Liu, L.; Han, J.; Xu, L.; Zhou, J.; Zhao, C.; Ding, S.; Shi, H.; Xiao, M.; Ding, L.; Ma, Z.; Jin, C.; Zhang, Z.; Peng, L.-M. Aligned, high-density semiconducting carbon nanotube arrays for high-performance electronics. *Science* **2020**, *368* (6493), 850–856.
- (6) Castro Neto, A. H.; Guinea, F.; Peres, N. M. R.; Novoselov, K. S.; Geim, A. K. The electronic properties of graphene. *Rev. Mod. Phys.* **2009**, *81* (1), 109.
- (7) Li, Z.; Qian, H.; Wu, J.; Gu, B.-L.; Duan, W. Role of symmetry in the transport properties of graphene nanoribbons under bias. *Phys. Rev. Lett.* **2008**, *100* (20), 206802.
- (8) Cresti, A.; Nemec, N.; Biel, B.; Niebler, G.; Triozon, F.; Cuniberti, G.; Roche, S. Charge transport in disordered graphene-based low dimensional materials. *Nano Res.* **2008**, *1* (5), 361–394.
- (9) Gui, G.; Li, J.; Zhong, J. Band structure engineering of graphene by strain: First-principles calculations. *Phys. Rev. B: Condens. Matter Mater. Phys.* **2008**, 78 (7), 075435.
- (10) Cao, M. S.; Shu, J. C.; Wang, X. X.; Wang, X.; Zhang, M.; Yang, H. J.; Fang, X. Y.; Yuan, J. Electronic structure and electromagnetic properties for 2D electromagnetic functional materials in gigahertz frequency. *Ann. Phys.* **2019**, *531* (4), 1800390.
- (11) Bolotin, K. İ.; Sikes, K. J.; Jiang, Z.; Klima, M.; Fudenberg, G.; Hone, J. e.; Kim, P.; Stormer, H. Ultrahigh electron mobility in suspended graphene. *Solid State Commun.* **2008**, 146 (9–10), 351–355
- (12) Son, Y.-W.; Cohen, M. L.; Louie, S. G. Half-metallic graphene nanoribbons. *Nature* **2006**, 444 (7117), 347–349.
- (13) Li, J.; Friedrich, N.; Merino, N.; de Oteyza, D. G.; Peña, D.; Jacob, D.; Pascual, J. I. Electrically Addressing the Spin of a Magnetic Porphyrin through Covalently Connected Graphene Electrodes. *Nano Lett.* **2019**, *19* (5), 3288–3294.
- (14) Chen, Y.-C.; Cao, T.; Chen, C.; Pedramrazi, Z.; Haberer, D.; de Oteyza, D. G.; Fischer, F. R.; Louie, S. G.; Crommie, M. F. Molecular bandgap engineering of bottom-up synthesized graphene nanoribbon heterojunctions. *Nat. Nanotechnol.* **2015**, *10* (2), 156–160.
- (15) Allen, M. J.; Tung, V. C.; Kaner, R. B. Honeycomb Carbon: A Review of Graphene. *Chem. Rev.* **2010**, *110* (1), 132–145.
- (16) Aviram, A.; Ratner, M. A. Molecular rectifiers. *Chem. Phys. Lett.* **1974**, 29 (2), 277–283.
- (17) Bumm, L.; Arnold, J.; Cygan, M.; Dunbar, T.; Burgin, T.; Jones, L.; Allara, D. L.; Tour, J. M.; Weiss, P. Are single molecular wires conducting? *Science* **1996**, *271* (5256), 1705–1707.
- (18) Reed, M. A.; Zhou, C.; Muller, C.; Burgin, T.; Tour, J. Conductance of a molecular junction. *Science* **1997**, 278 (5336), 252–254
- (19) Xu, B.; Tao, N. J. Measurement of single-molecule resistance by repeated formation of molecular junctions. *Science* **2003**, *301* (5637), 1221–1223.
- (20) Li, J.; Zhang, Z. H.; Zhang, J. J.; Tian, W.; Fan, Z. Q.; Deng, X. Q.; Tang, G. P. Spin polarization effects of zigzag-edge graphene electrodes on the rectifying performance of the D- σ -A molecular diode. *Org. Electron.* **2013**, *14* (3), 958–965.
- (21) Niu, L.-L.; Fu, H.-Y.; Suo, Y.-Q.; Liu, R.; Sun, F.; Wang, S.-S.; Zhang, G.-P.; Wang, C.-K.; Li, Z.-L. Doping-induced large spin-filter behavior and rectification behavior in zigzag graphene nano-ribbon junction. *Phys. E* **2021**, *128*, 114542.

- (22) Cai, Y.; Zhang, A.; Ping Feng, Y.; Zhang, C. Switching and rectification of a single light-sensitive diarylethene molecule sandwiched between graphene nanoribbons. *J. Chem. Phys.* **2011**, *135* (18), 184703.
- (23) Wan, H.; Zhou, B.; Chen, X.; Sun, C. Q.; Zhou, G. Switching, dual spin-filtering effects, and negative differential resistance in a carbon-based molecular device. *J. Phys. Chem. C* **2012**, *116* (3), 2570–2574
- (24) Hu, Z.-Y.; Xia, C.-J.; Tang, X.-J.; Zhang, T.-T.; Yu, J.; Liu, Y. Switching behavior induced by the orientation in triangular graphene molecular junction with graphene nanoribbons electrodes. *Optik* **2021**, 225, 165710.
- (25) Zhang, D.; Long, M.; Zhang, X.; Xu, H. High performance bipolar spin filtering and switching functions of poly-(terphenylene-butadiynylene) between zigzag graphene nanoribbon electrodes. *RSC Adv.* **2015**, *5* (117), 96455–96463.
- (26) Wang, M.; Li, C. M. Negative differential resistance in oxidized zigzag graphene nanoribbons. *Phys. Chem. Chem. Phys.* **2011**, *13* (4), 1413–1418.
- (27) Huang, J.; Wang, W.; Li, Q.; Yang, J. Negative differential resistance devices by using N-doped graphene nanoribbons. *J. Chem. Phys.* **2014**, *140* (16), 164703.
- (28) Liang, X.; Wi, S. Transport characteristics of multichannel transistors made from densely aligned sub-10 nm half-pitch graphene nanoribbons. *ACS Nano* **2012**, *6* (11), 9700–9710.
- (29) Novoselov, K. S.; Geim, A. K.; Morozov, S. V.; Jiang, D.; Zhang, Y.; Dubonos, S. V.; Grigorieva, I. V.; Firsov, A. A. Electric field effect in atomically thin carbon films. *Science* **2004**, *306* (5696), 666–669.
- (30) Zhang, K.; Fu, Q.; Pan, N.; Yu, X.; Liu, J.; Luo, Y.; Wang, X.; Yang, J.; Hou, J. Direct writing of electronic devices on graphene oxide by catalytic scanning probe lithography. *Nat. Commun.* **2012**, 3 (1), 1–6
- (31) Yao, Y.; Wang, C.; Zhang, G.; Ji, M.; Ho, K. A first-principles divide-and-conquer approach for electronic structure of large systems and its application to graphene nanoribbons. *J. Phys.: Condens. Matter* **2009**, *21* (23), 235501.
- (32) Brey, L.; Fertig, H. Electronic states of graphene nanoribbons studied with the Dirac equation. *Phys. Rev. B: Condens. Matter Mater. Phys.* **2006**, *73* (23), 235411.
- (33) Zhang, G.; Fang, X.; Yao, Y.-X.; Wang, C.; Ding, Z.; Ho, K.-M. Electronic structure and transport of a carbon chain between graphene nanoribbon leads. *J. Phys.: Condens. Matter* **2011**, *23* (2), 025302.
- (34) Yelin, T.; Korytár, R.; Sukenik, N.; Vardimon, R.; Kumar, B.; Nuckolls, C.; Evers, F.; Tal, O. Conductance saturation in a series of highly transmitting molecular junctions. *Nat. Mater.* **2016**, *15* (4), 444–449.
- (35) Zhao, S.; Wu, Q.; Pi, J.; Liu, J.; Zheng, J.; Hou, S.; Wei, J.; Li, R.; Sadeghi, H.; Yang, Y.; Shi, J.; Chen, Z.; Xiao, Z.; Lambert, C.; Hong, W.; et al. Cross-plane transport in a single-molecule two-dimensional van der Waals heterojunction. *Sci. Adv.* **2020**, *6* (22), No. eaba6714.
- (36) Liu, Y.; Ornago, L.; Carlotti, M.; Ai, Y.; El Abbassi, M.; Soni, S.; Asyuda, A.; Zharnikov, M.; van der Zant, H. S. J.; Chiechi, R. C. Intermolecular Effects on Tunneling through Acenes in Large-Area and Single-Molecule Junctions. *J. Phys. Chem. C* **2020**, *124* (41), 22776–22783.
- (37) Isshiki, Y.; Nishino, T.; Fujii, S. Electronic Structure and Transport Properties of Single-Molecule Junctions with Different Sizes of π -Conjugated System. *J. Phys. Chem. C* **2021**, *125* (6), 3472–3479.
- (38) Geng, Y.; Sangtarash, S.; Huang, C.; Sadeghi, H.; Fu, Y.; Hong, W.; Wandlowski, T.; Decurtins, S.; Lambert, C. J.; Liu, S.-X. Magic Ratios for Connectivity-Driven Electrical Conductance of Graphene-like Molecules. *J. Am. Chem. Soc.* **2015**, *137* (13), 4469–4476.
- (39) Sangtarash, S.; Huang, C.; Sadeghi, H.; Sorohhov, G.; Hauser, J.; Wandlowski, T.; Hong, W.; Decurtins, S.; Liu, S.-X.; Lambert, C. J. Searching the Hearts of Graphene-like Molecules for Simplicity, Sensitivity, and Logic. J. Am. Chem. Soc. 2015, 137 (35), 11425–11431.
- (40) Quinn, J. R.; Foss, F. W.; Venkataraman, L.; Hybertsen, M. S.; Breslow, R. Single-Molecule Junction Conductance through Diaminoacenes. *J. Am. Chem. Soc.* **2007**, *129* (21), 6714–6715.

- (41) Valdiviezo, J.; Rocha, P.; Polakovsky, A.; Palma, J. L. Nonexponential Length Dependence of Molecular Conductance in Acene-Based Molecular Wires. ACS Sens 2021, 6 (2), 477–484.
- (42) Civita, D.; Kolmer, M.; Simpson, G. J.; Li, A.-P.; Hecht, S.; Grill, L. Control of long-distance motion of single molecules on a surface. *Science* **2020**, 370 (6519), 957–960.
- (43) Andrei, E. Y.; MacDonald, A. H. Graphene bilayers with a twist. *Nat. Mater.* **2020**, *19* (12), 1265–1275.
- (44) Kim, G.; Ma, K. Y.; Park, M.; Kim, M.; Jeon, J.; Song, J.; Barrios-Vargas, J. E.; Sato, Y.; Lin, Y.-C.; Suenaga, K.; Roche, S.; Yoo, S.; Sohn, B.-H.; Jeon, S.; Shin, H. S. Blue emission at atomically sharp 1D heterojunctions between graphene and h-BN. *Nat. Commun.* **2020**, *11* (1), 5359.
- (45) Peller, D.; Kastner, L. Z.; Buchner, T.; Roelcke, C.; Albrecht, F.; Moll, N.; Huber, R.; Repp, J. Sub-cycle atomic-scale forces coherently control a single-molecule switch. *Nature* **2020**, *585* (7823), 58–62.
- (46) Li, Y.; Buerkle, M.; Li, G.; Rostamian, A.; Wang, H.; Wang, Z.; Bowler, D. R.; Miyazaki, T.; Xiang, L.; Asai, Y.; Zhou, G.; Tao, N. Gate controlling of quantum interference and direct observation of anti-resonances in single molecule charge transport. *Nat. Mater.* **2019**, *18* (4), 357–363.
- (47) Kilibarda, F.; Strobel, A.; Sendler, T.; Wieser, M.; Mortensen, M.; Trads, J. B.; Helm, M.; Kerbusch, J.; Scheer, E.; Gemming, S.; Gothelf, K. V.; Erbe, A. Single-Molecule Doping: Conductance Changed By Transition Metal Centers in Salen Molecules. *Adv. Electron. Mater.* **2021**, *7* (10), 2100252.
- (48) Wang, H. S.; Chen, L.; Elibol, K.; He, L.; Wang, H.; Chen, C.; Jiang, C.; Li, C.; Wu, T.; Cong, C. X.; Pennycook, T. J.; Argentero, G.; Zhang, D.; Watanabe, K.; Taniguchi, T.; Wei, W.; Yuan, Q.; Meyer, J. C.; Xie, X. Towards chirality control of graphene nanoribbons embedded in hexagonal boron nitride. *Nat. Mater.* **2021**, *20* (2), 202–207.
- (49) Huang, M. Z.; Dong, J. Q.; Wang, Z. Y.; Li, Y. C.; Yu, L.; Liu, Y. C.; Qian, G. M.; Chang, S. Revealing the electronic structure of organic emitting semiconductors at the single-molecule level. *Chem. Commun.* **2020**, *56* (94), 14789–14792.
- (50) Huang, M. Z.; Sun, M. J.; Yu, X.; He, S. H.; Liu, S. M.; Nau, W. M.; Li, Y. C.; Wu, T.; Wang, Y.; Chang, S.; He, J. Reliably Probing the Conductance of a Molecule in a Cavity via van der Waals Contacts. *J. Phys. Chem. C* **2020**, 124 (29), 16143–16148.
- (51) Huang, M.; Zhou, Q.; Liang, F.; Yu, L.; Xiao, B.; Li, Y.; Zhang, M.; Chen, Y.; He, J.; Xiao, S.; Chang, S. Detecting Individual Bond Switching within Amides in a Tunneling Junction. *Nano Lett.* **2021**, *21* (12), 5409–5414.
- (52) Huang, M.; Yu, L.; Zhang, M.; Wang, Z.; Xiao, B.; Liu, Y.; He, J.; Chang, S. Developing Longer-Lived Single Molecule Junctions with a Functional Flexible Electrode. *Small* **2021**, *17* (36), 2101911.
- (53) Yoshizawa, K.; Tada, T.; Staykov, A. Orbital Views of the Electron Transport in Molecular Devices. *J. Am. Chem. Soc.* **2008**, *130* (29), 9406–9413.
- (54) Yoshizawa, K. An Orbital Rule for Electron Transport in Molecules. *Acc. Chem. Res.* **2012**, *45* (9), 1612–1621.
- (55) Migita, T.; Shimizu, T.; Asami, Y.; Shiobara, J.-i.; Kato, Y.; Kosugi, M. The Palladium Catalyzed Nucleophilic Substitution of Aryl Halides by Thiolate Anions. *Bull. Chem. Soc. Jpn.* **1980**, *53* (5), 1385–1389
- (56) Goretta, S.; Tasciotti, C.; Mathieu, S.; Smet, M.; Maes, W.; Chabre, Y. M.; Dehaen, W.; Giasson, R.; Raimundo, J.-M.; Henry, C. R.; Barth, C.; Gingras, M. Expeditive Syntheses of Functionalized Pentahelicenes and NC-AFM on Ag(001). *Org. Lett.* **2009**, *11* (17), 3846–3849.
- (57) Pinchart, A.; Dallaire, C.; Van Bierbeek, A.; Gingras, M. Efficient formation of aromatic thiols from thiomethylated precursors. *Tetrahedron Lett.* **1999**, 40 (30), 5479–5482.
- (58) Meisner, J. S.; Ahn, S.; Aradhya, S. V.; Krikorian, M.; Parameswaran, R.; Steigerwald, M.; Venkataraman, L.; Nuckolls, C. Importance of Direct Metal $-\pi$ Coupling in Electronic Transport Through Conjugated Single-Molecule Junctions. *J. Am. Chem. Soc.* **2012**, *134* (50), 20440–20445.

- (59) Aradhya, S. V.; Meisner, J. S.; Krikorian, M.; Ahn, S.; Parameswaran, R.; Steigerwald, M. L.; Nuckolls, C.; Venkataraman, L. Dissecting Contact Mechanics from Quantum Interference in Single-Molecule Junctions of Stilbene Derivatives. *Nano Lett.* **2012**, *12* (3), 1643–1647.
- (60) Su, T. A.; Li, H.; Steigerwald, M. L.; Venkataraman, L.; Nuckolls, C. Stereoelectronic switching in single-molecule junctions. *Nat. Chem.* **2015**, *7* (3), 215–220.
- (61) Perrin, M. L.; Burzurí, E.; van der Zant, H. S. J. Single-molecule transistors. *Chem. Soc. Rev.* **2015**, 44 (4), 902–919.
- (62) Capozzi, B.; Xia, J.; Adak, O.; Dell, E. J.; Liu, Z.-F.; Taylor, J. C.; Neaton, J. B.; Campos, L. M.; Venkataraman, L. Single-molecule diodes with high rectification ratios through environmental control. *Nat. Nanotechnol.* **2015**, *10* (6), 522–527.
- (63) Isshiki, Y.; Matsuzawa, Y.; Fujii, S.; Kiguchi, M. Investigation on Single-Molecule Junctions Based on Current-Voltage Characteristics. *Micromachines* **2018**, *9* (2), 67.
- (64) Peskin, U. An introduction to the formulation of steady-state transport through molecular junctions. *J. Phys. B: At., Mol. Opt. Phys.* **2010**, 43 (15), 153001.
- (65) Mayor, M.; Weber, H. B.; Reichert, J.; Elbing, M.; von Hänisch, C.; Beckmann, D.; Fischer, M. Electric Current through a Molecular Rod—Relevance of the Position of the Anchor Groups. *Angew. Chem., Int. Ed.* **2003**, 42 (47), 5834–5838.
- (66) Solomon, G. C.; Herrmann, C.; Hansen, T.; Mujica, V.; Ratner, M. A. Exploring local currents in molecular junctions. *Nat. Chem.* **2010**, 2 (3), 223–228.
- (67) Gunasekaran, S.; Greenwald, J. E.; Venkataraman, L. Visualizing Quantum Interference in Molecular Junctions. *Nano Lett.* **2020**, 20 (4), 2843–2848.
- (68) O'Driscoll, L. J.; Bryce, M. R. Extended curly arrow rules to rationalise and predict structural effects on quantum interference in molecular junctions. *Nanoscale* **2021**, *13* (2), 1103–1123.